Article

Design and Control of Acetic Acid Dehydration Column with *p*-Xylene or *m*-Xylene Feed Impurity. 1. Importance of Feed Tray Location on the Process Design

Hsiao-Ping Huang, Hao-Yeh Lee, and Tang-Kai GauI-Lung Chien

Ind. Eng. Chem. Res., **2007**, 46 (2), 505-517 • DOI: 10.1021/ie060883o

Design and Control of Acetic Acid Dehydration Column with *p*-Xylene or *m*-Xylene Feed Impurity. 1. Importance of Feed Tray Location on the Process Design

Hsiao-Ping Huang, Hao-Yeh Lee, and Tang-Kai Gau

Department of Chemical Engineering, National Taiwan University, Taipei 106, Taiwan

I-Lung Chien*

Department of Chemical Engineering, National Taiwan University of Science and Technology, Taipei 106, Taiwan

In the production of aromatic acids, such as terephthalic acid and isophthalic acid, tiny amounts of reactant *p*-xylene or *m*-xylene may also enter into the acetic acid dehydration column through the feed stream. In this work, the process design flow sheets both with and without these tiny impurities are considered. For the case with one of these tiny impurities in the feed stream in combination with a high-purity specification for the bottom stream, a side stream is necessary to purge the impurity; otherwise, accumulation of the impurity will occur inside the column. If only the optimum side stream location and its flow rate are considered in the optimization search, it is found that the total annual cost and the operating cost of this acetic acid dehydration column become much higher by just adding a tiny amount of *p*-xylene or *m*-xylene in the feed stream, compared to the no-impurity case. With careful reselection of the feed tray location, significant total annual cost and energy savings for the operation of this column can be realized. A separate case with lower bottom product specification has also been investigated. In this case, the side stream is not necessary because this impurity can leave the system from the bottom stream. The process design investigation reveals that the selection of the feed tray location is also extremely important. The distillation path of the column composition profile for the optimum design follows a path with more *p*-xylene in the bottom part of the column. This desirable distillation path should be maintained even though various disturbance changes inevitably could enter into the column system.

1. Introduction

Acetic acid (HAc) dehydration is an important operation in the production of aromatic acids, such as terephthalic acid and isophthalic acid,[1,2] or in the manufacture of cellulose acetate. To make the separation easier, an entrainer is often introduced into the system. In a review paper, Othmer[3] described an azeotropic distillation system containing a dehydrating column, a decanter, and a water column for the separation of HAc and water. The entrainer used before 1932 was ethylene dichloride, and later *n*-propyl acetate and *n*-butyl acetate were used to reduce the organic reflux and heat duty used in the dehydrating column. In a paper by Pham and Doherty,[4] examples of the use of ethyl acetate,[5] *n*-propyl acetate,[6] or *n*-butyl acetate as the entrainer are listed in a table of examples of heterogeneous azeotropic separations. Siirola[7] uses HAc dehydration as an example to demonstrate a systematic process synthesis technique for the conceptual design of a process flow sheet. Ethyl acetate is used as the entrainer in that paper to design a complete HAc dehydration process with multiple-effect azeotropic distillation and heat integration. Wasylkiewicz et al.[8] proposed using a geometric method for the optimum design of a HAc dehydrating column with *n*-butyl acetate as the entrainer. Recently, Chien et al.[9] studied the design and control of a HAc dedydration system via heterogeneous azeotropic distillation. A suitable entrainer of isobutyl acetate (IBA) was selected from three candidate acetates by total annual cost (TAC) analysis.

In the previous studies, only three components (HAc, H_2O, and the entrainer) in the heterogeneous distillation column were focused. However, in the production of aromatic acids, HAc is used as a solvent in the terephthalic acid and isophthalic acid processes. A terephthalic acid or isophthalic acid slurry in HAc solvent is produced by oxidizing *p*-xylene (PX) or *m*-xylene (MX), removing H_2O by evaporation of a stream of H_2O and HAc, and returning HAc to the oxidation step.[1,2] To recover HAc as a cyclic solvent stream, a HAc dehydrating column is necessary. However, tiny amounts of one reactant may also enter this HAc dehydration column through the feed stream.

For the feed stream with impurities, Chien et al.[10] studied the design and operation of an industrial column for HAc dehydration process with five feed streams. The entrainer used for this industrial column to aid the separation was also IBA. In that paper, optimum design of the side stream location and its flow rate were performed and an automatic purging strategy was proposed to prevent accumulation of an impurity (not specified for proprietary reasons) inside the column. However, the effect of changing the feed tray location was not investigated in that paper.

In this work, a HAc dehydration column via a heterogeneous azeotropic column system with and without an impurity in the feed stream will be thoroughly studied. The entrainer used in the study is IBA, and the impurity in the feed stream is assumed to be PX or MX, which are reactants commonly used in terephthalic acid and isophthalic acid plants. Three optimum design processes will be studied. The first one assumes that the tiny amount of PX or MX is not considered in the feed stream.

* To whom correspondence should be addressed. Tel.: +886-2-2737-6652. Fax: +886-2-2737-6644. E-mail: chien@ch.ntust.edu.tw.

10.1021/ie060883o CCC: $37.00
Published on Web 12/15/2006

Table 1. NRTL Model for HAc−IBA−H_2O with PX Impurity[a]

component *i*	IBA	HAc	IBA	HAc	H_2O	IBA
component *j*	H_2O	H_2O	HAc	PX	PX	PX
a_{ij}	0	0	0	0	5.918179	0
a_{ji}	0	0	0	0	−6.03013	0
b_{ij}	489.6086	−211.31	194.416	466.2167	747.8602	1025.975
b_{ji}	1809.079	652.995	90.2676	215.8257	2909.308	−724.011
c_{ij}	0.250501	0.3	0.3	0.30003	0.162808	0.1017

[a] Aspen Plus NRTL, $\ln \gamma_i = \frac{\sum_j x_j \tau_{ji} G_{ji}}{\sum_k x_k G_{ki}} + \sum_j \frac{x_j G_{ij}}{\sum_k x_k G_{kj}} \left[\tau_{ij} - \frac{\sum_m x_m \tau_{mj} G_{mj}}{\sum_k x_k G_{kj}} \right]$, where $G_{ij} = \exp(-\alpha_{ij}\tau_{ij})$; $\tau_{ij} = a_{ij} + b_{ij}/T$; $\alpha_{ij} = c_{ij}$, $\tau_{ii} = 0$, and $G_{ii} = 1$.

Table 2. Experimental and Predicted Values of Azeotropes for HAc−IBA−H_2O with PX Impurity at Pressure of 1 atm

components	exptl composition (mol %)	exptl temp (°C)	calcd composition (mol %)	calcd temp (°C)
HAc−PX (homogeneous)	81.97, 18.03	115.25	80.83, 19.17	115.22
H_2O−PX (heterogeneous)	74.5, 25.5	92	75.74, 24.26	92.39
IBA−H_2O (heterogeneous)	39.04, 60.96	87.45	36.76, 63.24	87.72
HAc−IBA[a] (homogeneous)	24.18, 75.82	117.00[b]	15.8, 84.2	117.12
HAc−IBA[a] (homogeneous)	62.08, 37.92	117.00[c]	56.3, 43.7	117.01

[a] Burguet et al.[13] [b] At 101.13 kPa. [c] At 101.32 kPa.

The optimized design and operating variables include the column total stages, feed tray location, and the aqueous reflux ratio. The column total stages and the feed tray location obtained from this optimum search will be used in the second study with tiny amounts of PX or MX entering the column through the feed stream. The optimal side stream location and its flow rate will be investigated. In the third design also with the impurity in the feed stream, besides the side stream location and its flow rate, the feed tray location will also be adjusted in this case. The results of the above three cases will be compared.

The organization of this paper is as follows. Section 2 will describe the thermodynamic properties of these two HAc dehydration systems with PX or MX as impurity. The validation of thermodynamic models with vapor−liquid and liquid−liquid equilibrium data and boiling points of components and azeotropes are illustrated for these systems. Section 3 will obtain the optimum design of the three HAc dehydration column systems with and without feed impurity as described above. TAC will be used to determine the optimum design flow sheets. In this section, an additional design with lower purity specification of the bottom product will also be studied. In this case, the side stream is not necessary to satisfy the top and bottom specifications. However, this design flow sheet without side stream may be vulnerable with wider feed impurity variations which can easily occur in industry. Section 4 will discuss the behavior due to different feed tray locations on the column design. The distillation path of the column composition profile for the proposed optimum design will be compared to that of the case with the feed tray location fixed at the original optimum design without this tiny impurity. Some concluding remarks will be given in section 5.

2. Thermodynamic Models

There are fewer thermodynamic data for the HAc−H_2O−IBA system with PX or MX component. Especially for HAc−H_2O−IBA with MX impurity system, only azeotrope experimental data were found from Gmehling.[11] In both of the two four-component systems, there are three azeotropes including one homogeneous azeotrope and two heterogeneous azeotropes. HAc−IBA−H_2O with PX impurity has a homogeneous azeotrope of HAc−PX and heterogeneous azeotropes of H_2O−PX and IBA−H_2O. HAc−IBA−H_2O with MX impurity has similar azeotropic behavior including a homogeneous azeotrope of HAc−MX and heterogeneous azeotropes of H_2O−MX and IBA−H_2O. In papers by Christensen and Olson[12] and Burguet et al.,[13] double homogeneous azeotropes in the HAc−IBA binary system were found. This information will also be incorporated into our thermodynamic model.

To accurately represent the overall system, selections of the form of the thermodynamic model and of its appropriate parameters are very important. The thermodynamic model parameters are obtained to fit the vapor−liquid and liquid−liquid equilibrium data. For these two systems, only the HAc−IBA−H_2O system with PX impurity has enough data for thermodynamic model regression. In this paper, a liquid activity coefficient model was used for the description of phase equilibrium. A suitable NRTL (nonrandom two-liquid) model parameter set has been established with prediction of the compositions and temperatures for the azeotropes in this system. Vapor association of HAc due to dimerization has also been included by using the second virial coefficient of the Hayden−O'Connell[14] model in the vapor phase. The Aspen Plus built-in association parameters are employed to compute fugacity coefficients. The NRTL model parameters for the PX as impurity system are regressed using the maximum likelihood method with HAc−IBA binary vapor−liquid equilibrium (VLE) data from Burguet et al.,[13] H_2O−PX binary liquid−liquid equilibrium (LLE) data from Jou and Mather,[15] and other binary and ternary VLE and VLLE data from Gmehling and Onken.[16] The complete NRTL model parameter set can be found in Table 1, and the predicted azeotropic compositions and temperatures in comparison with the experimental data from Gmehling[11] and Burguet et al.[13] can be found in Table 2. The computed azeotropic compositions and temperatures agree very well with the experimental data. The binary VLE $x-y$ and $T-x-y$ diagrams for the refitted HAc−H_2O, IBA−PX, and HAc−PX pairs are shown in Figure 1. The LLE curve for the ternary system of HAc−H_2O−IBA is shown in Figure 2. Notice that the thermodynamic model parameters used in this paper predicted VLE and LLE quite well in comparison with the experimental data.

Since there are not enough data for the system of HAc−H_2O−IBA with MX as impurity, the parameters in HAc−MX,

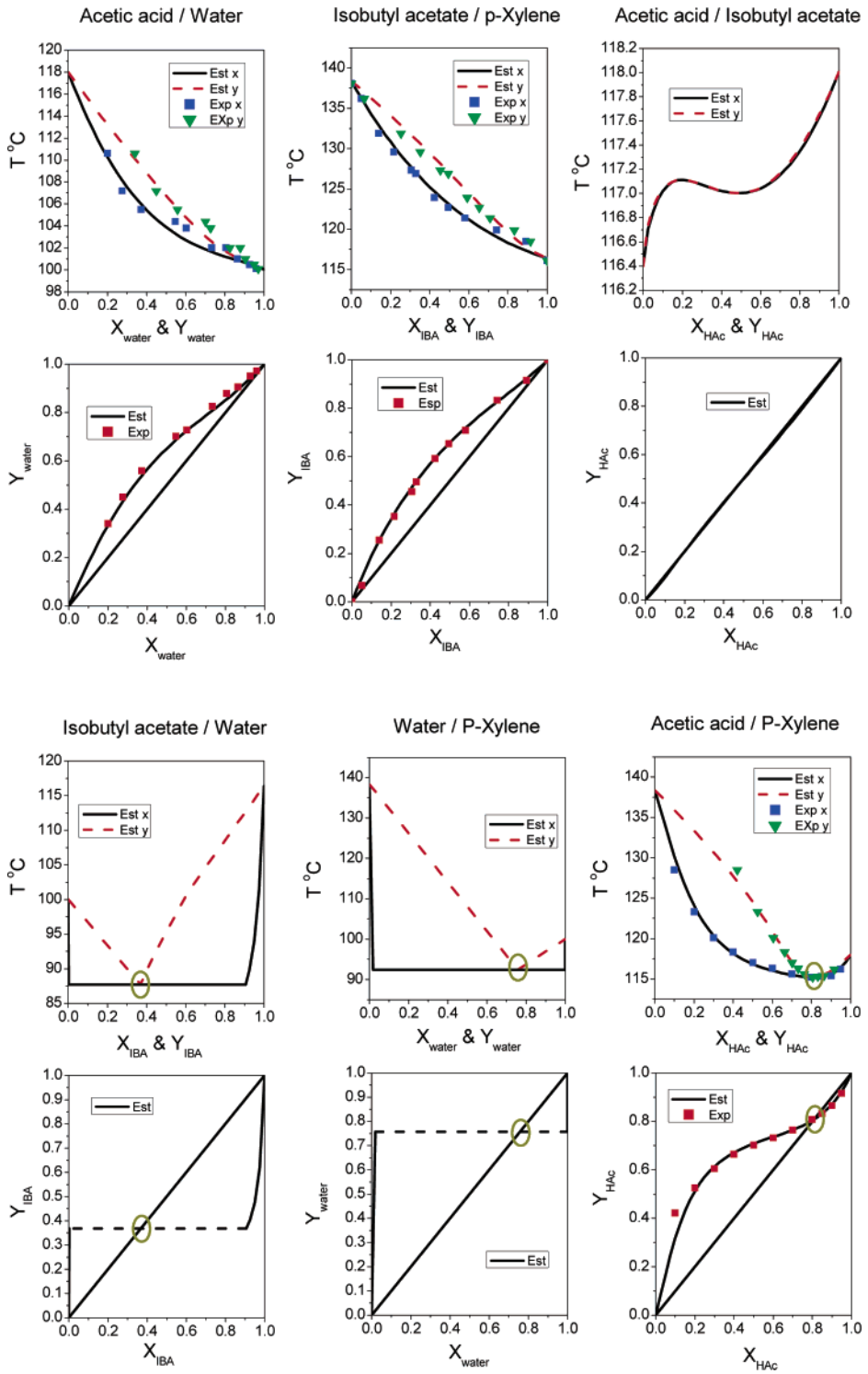

Figure 1. *T*−*x*−*y* and *x*−*y* experimental and predicted diagrams for PX impurity system.

H_2O−MX, and IBA−MX binary pairs are adopted from the Aspen Plus default built-in values. The prediction of azeotropes for this system again has to be validated with experimental data from Gmehling[11] and Burguet et al.[13] Reasonably good predictions of the azeotropic temperatures and compositions are obtained.

For the HAc−H_2O−IBA system with PX as impurity, the temperatures of the normal boiling points of the pure components can be sorted as follows:

$$H_2O\ (100.02\ °C) < IBA\ (116.4\ °C) < HAc\ (118.01\ °C) < PX\ (138.37\ °C)$$

From azeotropic temperatures in Table 2 in comparison with the above boiling points, the PX impurity has the maximum temperature and the IBA−H_2O azeotrope has the minimum temperature of the system. For the HAc−H_2O−IBA system with MX as impurity, the same behavior with MX impurity with the maximum temperature and IBA−H_2O azeotrope with the minimum temperature of the system has been found. Because similar thermodynamic properties are observed on both systems, the same process design procedure should apply to both systems.

From the above sorting of the normal boiling point temperatures of all the pure components and azeotropes, one would

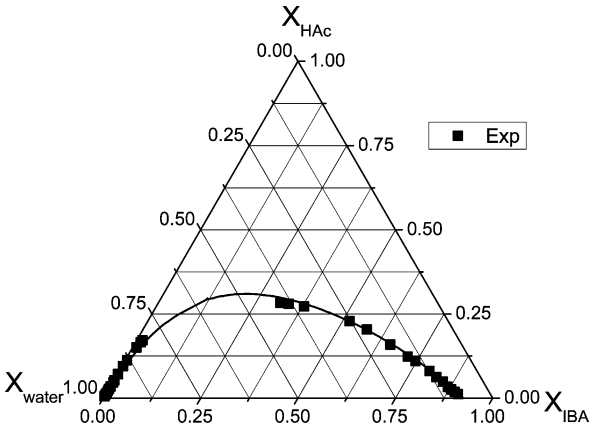

Figure 2. LLE experimental and predicted diagram for the ternary system of HAc−IBA−H_2O.

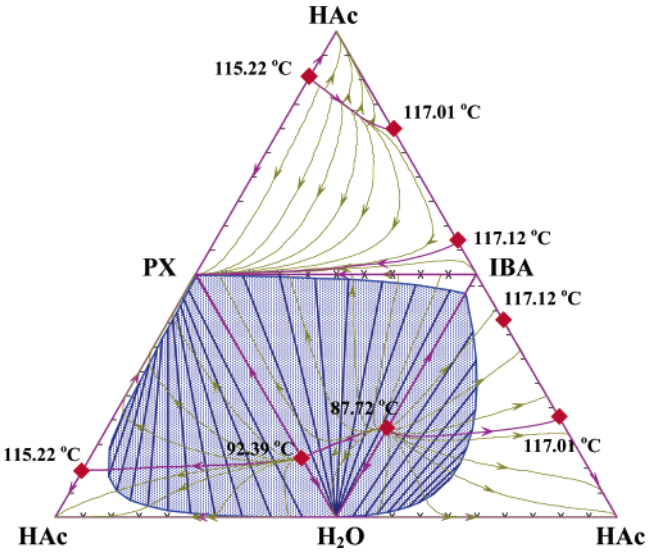

Figure 3. Composite RCMs for the four-component system.

think that for these two four-component systems the top vapor of the heterogeneous azeotropic column could be designed to be the IBA−H_2O azeotrope while the bottoms could be the pure PX or MX component. This design will defeat the purpose of producing pure HAc at the bottoms of this column.

We will use the four-component system with impurity PX as an example to demonstrate the conceptual design of the heterogeneous azeotropic column with feed impurity. The following display of the residue curve maps of quaternary mixtures put four ternary residue curve maps together into a composite diagram like the one in Figure 3. This diagram method was used in four-component reactive distillation processes by Tang et al.[17] In Figure 3, LLE binodal curves at 40 °C with tie lines, distillation boundaries, and azeotropic information are shown. Three LLE regions are found in the HAc−H_2O−IBA, H_2O−IBA−PX, and HAc−H_2O−PX ternary systems.

From the design principle of this separation system, the column top vapor should be near the IBA−H_2O azeotrope while the bottoms is at the pure HAc corner. The way to do this is to keep the column composition on the bottom side of the distillation boundaries in Figure 3. The first distillation boundary is from the PX−HAc azeotrope to the PX−H_2O azeotrope, the second distillation boundary is from the PX−H_2O azeotrope to the IBA−H_2O azeotrope, and the third distillation boundary is from the IBA−H_2O azeotrope to the IBA−HAc azeotrope at 117.01 °C. If the column is designed this way, the bottom product of pure PX can be avoided.

Another way to view the distillation regions of this quaternary system is from the method by Pöpken and Gmehling.[18] Figure 4 shows the two distillation regions of this quaternary system. The column should be operated in the region where the heaviest singular point is HAc and the lightest singular point is the heterogeneous azeotrope of IBA−H_2O. In this region, there is no way to produce pure PX or MX at the column bottoms. The column composition profile for the four-component system will be shown later.

3. Optimum Design of HAc Dehydration Column

3.1. Steady-State Design without Feed Impurity (Case 1). In this case with only three components of HAc, IBA, and H_2O, feed stream without impurity is assumed. In this study, the feed stream is assumed to contain equal moles of HAc and H_2O, and the flow rate of the total feed stream is 100 kmol/h. The entrainer IBA is introduced into the column through an organic reflux stream. Because of the addition of the entrainer, an IBA−H_2O heterogeneous azeotrope with minimum temperature of the system will be obtained at the top of the column. This top vapor stream with the heterogeneous azeotrope, after cooling to 40 °C at the decanter, will naturally split into two liquid phases. The organic phase containing mostly IBA can be totally refluxed back to the column. Part of the aqueous phase flow is also refluxed back to the column for higher purity with the rest leaving the system as wastewater stream. Since there is no feed impurity, the column bottoms without question will be HAc, which has the maximum boiling point temperature of this ternary system.

The process flow sheet can be seen in Figure 5. The product specifications are 99.9 mol % HAc recovered from the column bottoms and high purity water stream containing only 0.1 mol % HAc withdrawn from the decanter aqueous outlet stream. In the process simulation, the bottom product specification is set by varying the reboiler duty and the aqueous outlet product specification is set by varying the entrainer makeup flow rate.

There are three design variables yet to be determined in this flow sheet which can be optimized. The design variables are the column total stages, feed tray location, and the aqueous reflux fraction. The optimization procedure is to find the minimized total annual cost (TAC) by varying these three design variables as shown in the following:

(1) Guess the total number of stages.

(2) Guess the feed tray location.

(3) Guess the aqueous reflux fraction.

(4) Change the reboiler duty and the entrainer makeup flow rate until the two product specifications can be met.

(5) Go back to (3) and change the aqueous reflux fraction until TAC is minimized.

(6) Go back to (2) and change the feed tray location until TAC is minimized.

(7) Go back to (1) and change the total number of stages until TAC is minimized.

The optimization method is based on the sequential iterations with each design variable. The method is easy to execute and has physical meanings. However, it is rather time-consuming when the numbers of design variables become large in a plantwide optimization.

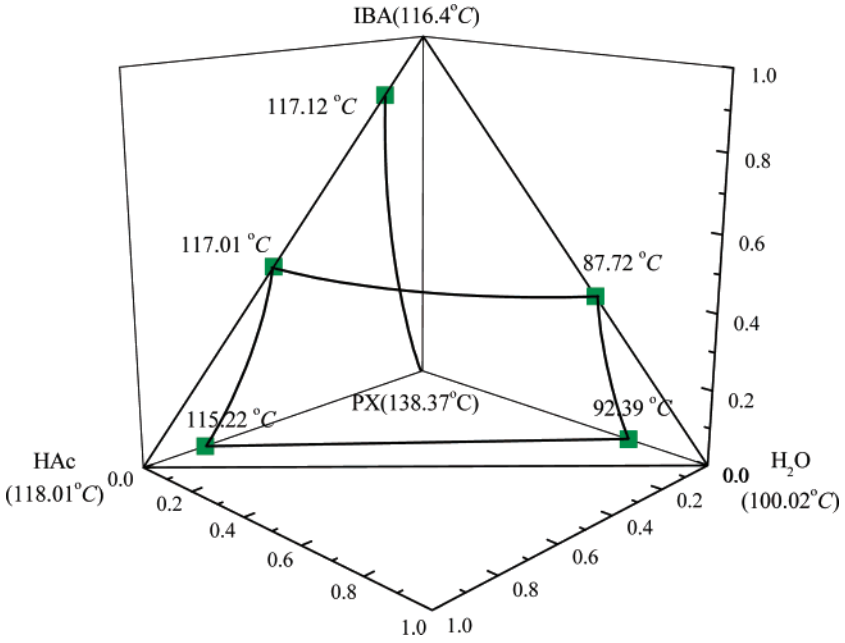

Figure 4. Three-dimensional plot showing distillation regions for the quaternary system.

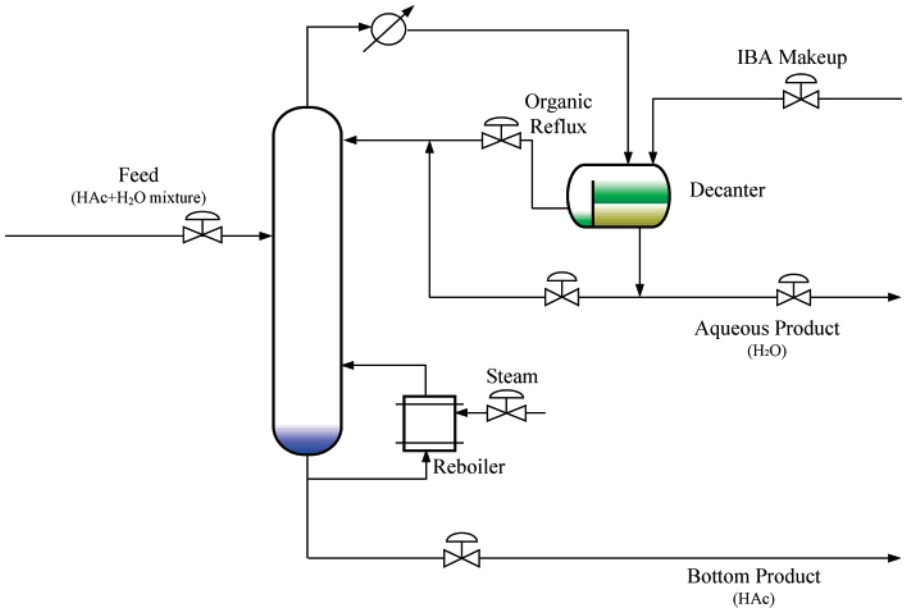

Figure 5. Process flow sheet for case 1.

The TAC as the following is evaluated for the optimal design:

$$\text{TAC} = \text{makeup cost} + \text{operating cost} + (\text{capital cost/payback period}) \quad (1)$$

where the makeup cost is calculated by the amount of makeup IBA entrainer, the operating cost includes the costs of steam and cooling water, the capital cost covers the costs of the column, trays, and two heat exchangers, and the payback period is assumed to be 3 years. The wastewater treatment cost is assumed to be negligible in the overall TAC.

Figure 6a shows that the minimized TAC can be found for a particular total number of stages by varying aqueous reflux flow and feed tray location with the two product specifications fixed. With a similar optimization search at other total stages, the overall minimized TAC can be found as in Figure 6b with column total stages of 39 (not including reboiler), feed tray location at the ninth stage, and the aqueous reflux fraction set at 0.11. The results of this case are given in Table 3, with the developed process flow sheet and detailed information of each stream is summarized in Figure 7. The temperature and composition profiles of this optimized flow sheet are shown in Figure 8.

From thermodynamic properties in section 2, the heterogeneous azeotrope IBA−H_2O will form at the column top. Based on the prediction of the thermodynamic model, the phase split phenomenon can be observed near the column top in the HAc−IBA−H_2O system. Figure 8 also displays the region of phase split from the first to fourth stages, and the results will be compared with the following simulations by considering impurity in the feed stream.

3.2. Steady-State Design with Feed Impurity. According to Chien et al.,[10] the HAc dehydration column with methyl acetate and some unknown impurities was studied. That study represented that if the design is based on the case without

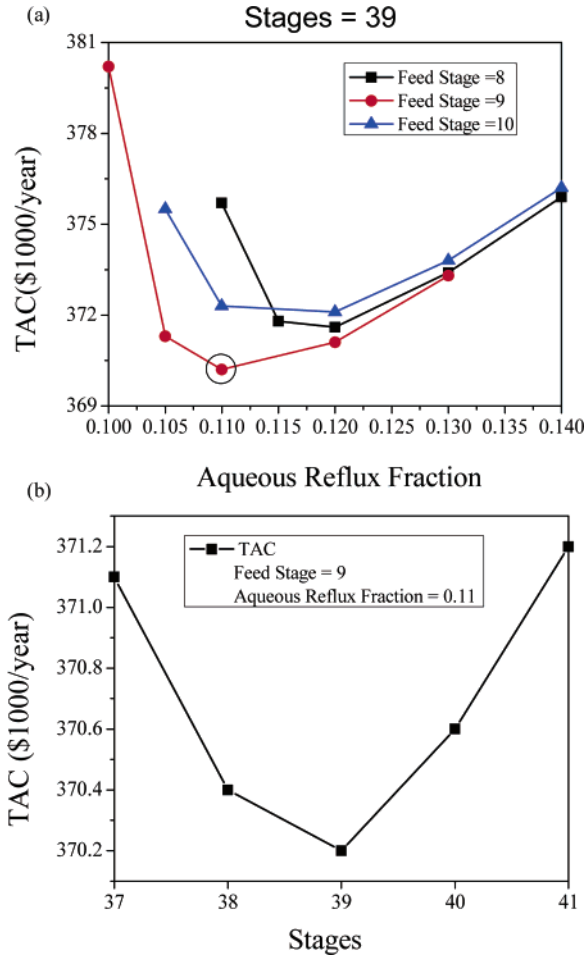

Figure 6. (a) Minimized TAC for a particular total number; (b) overall optimized results of TAC without feed impurity.

impurity, even with only an addition of a tiny impurity into the feed stream, the impurity will be accumulated inside the column. This will cause the overall control strategy to become invalid. Thus, the side stream flow is needed to purge the impurity inside the column.

3.2.1. Side Stream Location and Its Flow Rate as the Optimized Variables (Case 2). In the production of terephthalic acid or isophthalic acid, tiny amounts of reactant PX or MX may also enter this HAc dehydration column as impurity through the feed stream. In this second case with feed impurity, the same total feed stream flow rate 100 kmol/h as in case 1 is considered, and feed composition of 50 mol % H_2O, 49.9 mol % HAc, and 0.1 mol % PX or MX is assumed. From the analysis in section 2, the impurity should be able to draw out of the column through column bottoms if the column has a lower bottom purity specification. However, the bottom product specification is set to be 99.9 mol % HAc to avoid unwanted water from entering this bottom recycle stream. From a simple material balance calculation, the 0.1 mol % impurity in the feed stream cannot be totally drawn out from the column bottoms. Because the PX or MX is the heaviest component in the system which is negligible in the column top vapor stream, a side stream is necessary to purge this impurity; otherwise, accumulation of the impurity will occur inside the column.

Intuitive design thinking is to just use the optimum total stages and feed tray location obtained from the above no-impurity case and then investigate the optimal side stream flow rate and its location via TAC analysis. The merit of this design thinking is that the same column design can be suited for both the no-impurity case and the with tiny impurity case.

The optimization procedure is to fix the total stages at 39 (not counting reboiler) and the feed tray location at the ninth stage, and to vary the side stream location and its flow rate. Again, the bottom product specification is set by varying the reboiler duty and the aqueous outlet product specification is set by varying the entrainer makeup flow rate. For each simulation run, the aqueous reflux fraction that gives the lowest TAC is selected. The optimization procedure is as follows:

(1) Guess the side stream location.
(2) Guess the side stream flow rate.
(3) Guess the aqueous reflux fraction.
(4) Change the reboiler duty and the entrainer makeup flow rate until the two product specifications can be met.
(5) Go back to (3) and change the aqueous reflux fraction until TAC is minimized.
(6) Go back to (2) and change the side stream flow rate until TAC is minimized.
(7) Go back to (1) and change the side stream location until TAC is minimized.

The TAC formula for this case, case 2, is modified as the following equation by including an additional term to reflect the loss of HAc and IBA through the side stream.

$$\text{TAC} = \text{makeup cost} + \text{operating cost} + (\text{capital cost/payback period}) + \text{loss cost} \quad (2)$$

Figure 9 shows such simulation runs with side stream for the PX impurity system. For each side stream location, the aqueous reflux fraction and particular side stream flow rate will be selected with the total stages fixed at 39 and feed tray location fixed at the ninth stage. Doing similar runs at various side stream locations, the optimized result is found by the minimum TAC from this figure. Figure 9 shows that the optimum location of the side stream is at the 21st stage and its flow rate is at 0.7 kmol/h. The optimized configuration and detailed column flow sheet with stream information are summarized in Figure 10. For the system with MX as impurity, a similar optimization procedure is used which obtains the results that the side stream location and its flow rate are the same as the system with PX as impurity. The only difference in the two systems is that the aqueous reflux fractions are different by a little from 0.42 to 0.41 for the PX and MX systems, respectively.

Comparing the process configurations of case 1 with case 2, except for additional side stream flow, the major differences of these two cases are that the column reboiler duties as well as the organic and aqueous reflux flow rates need to be increased significantly for the case with impurity. From Figures 7 and 10, the organic and aqueous reflux flow rates of case 2 need to be increased to over 1.4 and 5 times, respectively, compared to case 1. The reboiler duty also needs to be increased over 50% compared to case 1.

According to the optimization steps, the product specification of the aqueous phase outlet composition is set by the entrainer makeup flow rate. However, the other important variable affecting the column top outlet compositions is the aqueous reflux flow rate. Since the vapor composition at the column top is designed to be near the H_2O-IBA azeotrope in order to split into two phases in the decanter, either larger entrainer makeup flow rate or larger aqueous reflux flow rate is needed to decrease HAc in the top aqueous outlet composition at its specification of 0.1 mol %. From the TAC analysis, larger

Table 3. TAC and Other Results for Cases 1−3[a]

	case 1	case 2		case 3	
	without impurity	MX impurity	PX impurity	MX impurity	PX impurity
TAC [$1000/year]	370.2 (base case)	553.1	559.6	436.8	438.3
operating cost [$1000/year]	106.7	161.2	163.8	129.3	133.4
feed location	9	9	9	23	24
side stream flow [kmol/h]		0.7	0.7	0.18	0.20
side stream location		21	21	17	18
reboiler duty [kW]	1113.68	1682.78	1710.80	1349.34	1393.48

[a] Bottom HAc = 99.9 mol %; top HAc = 0.1 mol %; total stages = 40.

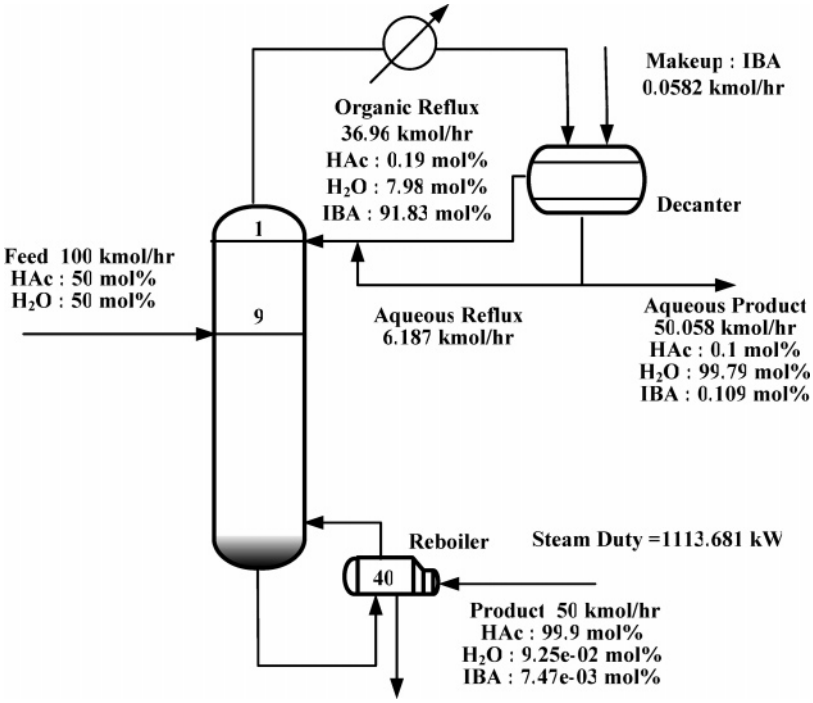

Figure 7. Optimized base case condition without impurity.

aqueous reflux flow rate can let the makeup flow rate not to be increased as much, thus reducing the makeup cost as needed. However, larger aqueous reflux flow rate will increase the column internal flow to cause larger reboiler duty and the required column diameter. In other words, the makeup cost will reduce with the tradeoff of larger reboiler duty and bigger column. The larger aqueous reflux flow rate required for case 2 implies that if the system has the same reboiler duty, aqueous reflux flow rate, and makeup flow rate as in case 1, the vapor compositions at the column top should be far from the H_2O−IBA azeotropic compositions. From the result of optimum flow sheets in Figures 7 and 10, one observes the economic tradeoff of this system from TAC analysis making the aqueous reflux flow rate to be increased with a much greater rate than the increasing rate of the entrainer makeup flow rate.

Notice also from these simulations that the design variables of the side stream flow rate in both systems are significantly more important than the side stream location. From Figure 9, a larger TAC difference is easily observed for the side stream flow rate from 0.6 to 0.8 kmol/h. Almost $\$1.0 \times 10^4$ TAC difference is observed with only 0.1 kmol/h difference in the side stream flow rate. However, under the same side stream flow rate, the results of TAC difference are much less with the difference of the side stream location.

The temperature and composition profiles for both the PX and MX impurities of case 2 are shown in Figure 11. Notice immediately that the systems with PX or MX as impurity exhibit almost the same behavior. From the composition profiles, PX or MX component has its highest fraction of about 0.21 at the eighth stage. However, the composition of the impurity drops sharply to about 0.1 at the ninth stage because of feed stream into the column. The impurity composition remains at this level with a slight increase until the tray for the side stream location. Below the tray for the side stream location, because this impurity is removed from the system, the impurity composition drops significantly to a negligible level. It is easy to observe that these heavy components of PX or MX affect the composition profiles significantly compared with case 1 even with only a tiny amount entering the column from the feed stream. Another effect of these impurities is phase splitting inside the column. From Figure 11, the number of trays exhibiting phase splitting phenomena in the column is extended from 4 to 21 stages showing a dramatic difference compared to case 1.

The results of TAC and reboiler duty information are given in Table 3. For PX impurity system, in comparing the base case conditions of Figures 7 and 10, it is found that the reboiler duty is changed from 1113.68 to 1710.80 KW, a 53.6% increase in this energy cost. The TAC is changed from $\$370.2 \times 10^3$ to $\$559.5 \times 10^3$ (a 51.1% increase), and the operating cost is changed from $\$106.7 \times 10^3$ to $\$163.8 \times 10^3$ (a 53.5% increase). For MX impurity system with similar results, the reboiler duty is changed from 1113.68 to 1682.78 KW (a 51.1% increase) in this energy cost. The TAC is changed from $\$370.2 \times 10^3$ to $\$553.1 \times 10^3$ (a 49.4% increase), and the operating cost is changed from $\$106.7 \times 10^3$ to $\$161.2 \times 10^3$ (a 51.1% increase). This shows a dramatic difference of the operating cost in the

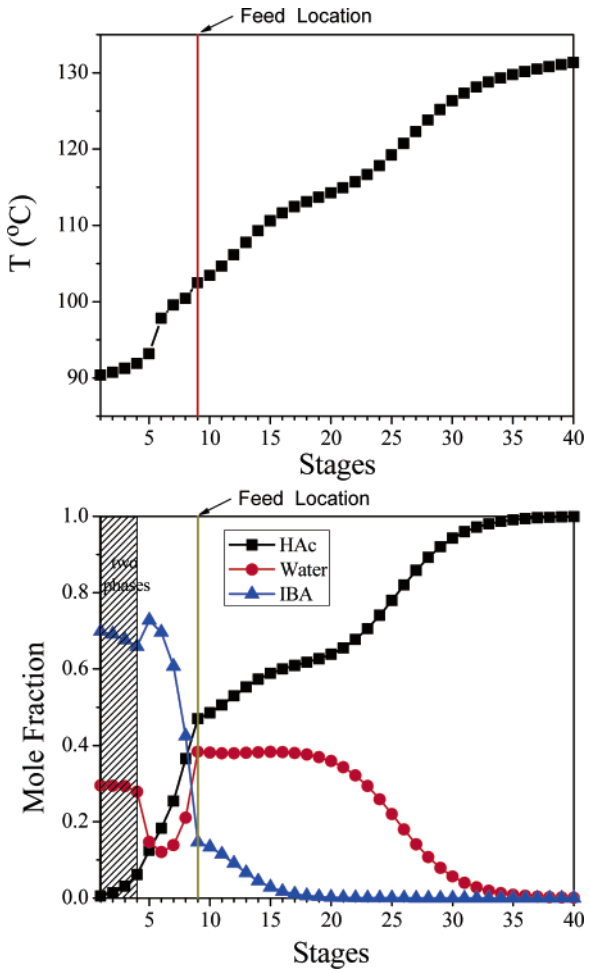

Figure 8. Temperature and liquid composition profiles for case 1.

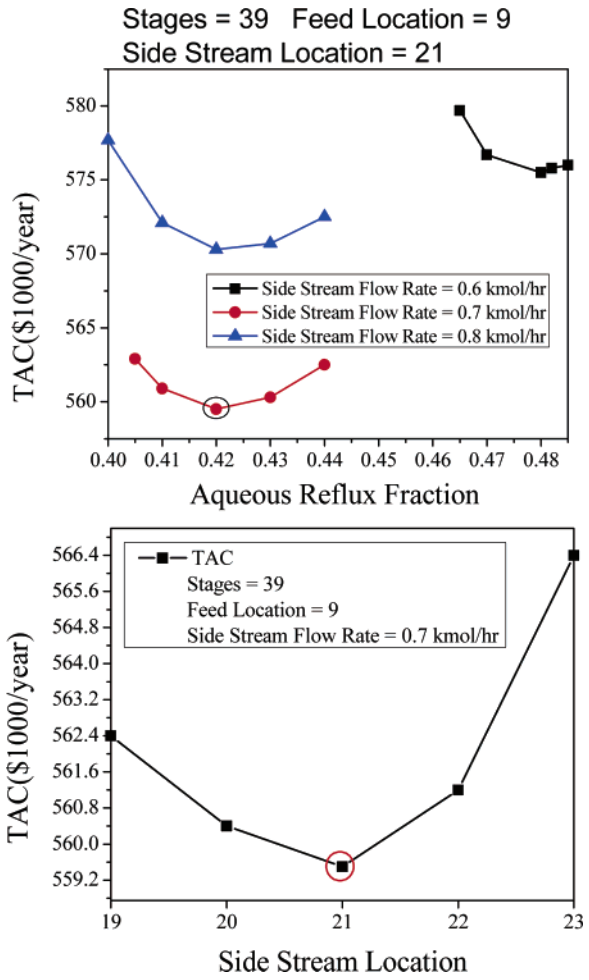

Figure 9. Optimized results with feed location at the ninth stage (PX feed impurity system).

base case conditions by just adding 0.1 mol % PX or MX feed impurity into this column.

3.2.2. With Feed Tray Location as the Additional Optimized Variable (Case 3). If additionally the feed tray location can be considered another optimized variable in the overall optimization procedure, the base case condition becomes very different from that of Figure 10. Considering feed tray location as another optimized variable does not defeat the original purpose of operating this column under both "without feed impurity" and "with feed impurity" cases. The total number of stages, feed stream conditions, and product specifications are fixed the same as in the previous case.

The optimization procedure will be more complicated by adding one more design variable in the search algorithm.

(1) Guess the feed location.

(2) Guess the side stream location.

(3) Guess the side stream flow rate.

(4) Guess the aqueous reflux fraction.

(5) Change the reboiler duty and the entrainer makeup flow rate until the two product specifications can be met.

(6) Go back to (4) and change the aqueous reflux fraction until TAC is minimized.

(7) Go back to (3) and change the side stream flow rate until TAC is minimized.

(8) Go back to (2) and change the side stream location until TAC is minimized.

(9) Go back to (1) and change the feed location until TAC is minimized.

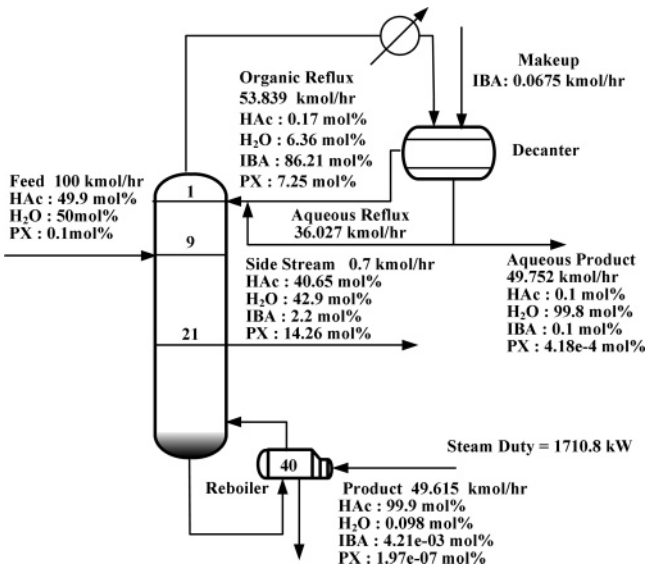

Figure 10. Process configuration with feed location at the ninth stage (PX feed impurity system).

Although only one design variable is added, the optimization procedure needs two more steps and one more loop iteration than that of case 2. For this case, basically the overall optimization procedure as in section 3.2.1 can be followed to find the design condition with the lowest TAC at a particular feed tray location. Then, this procedure is repeated to find the

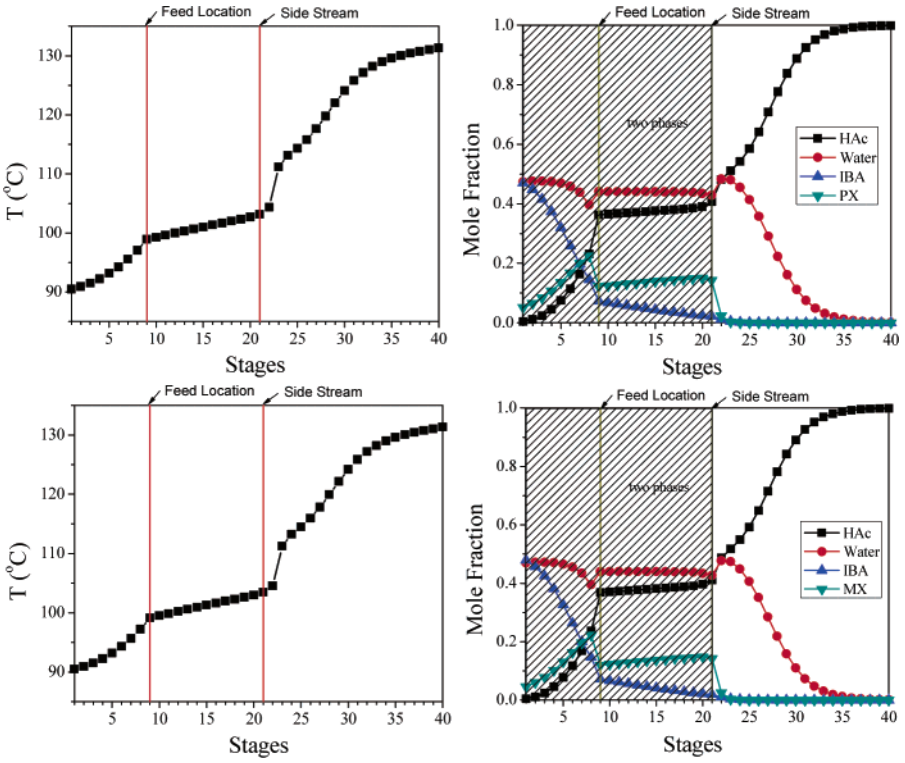

Figure 11. Temperature and liquid composition profiles for PX and MX impurity cases without changing feed location.

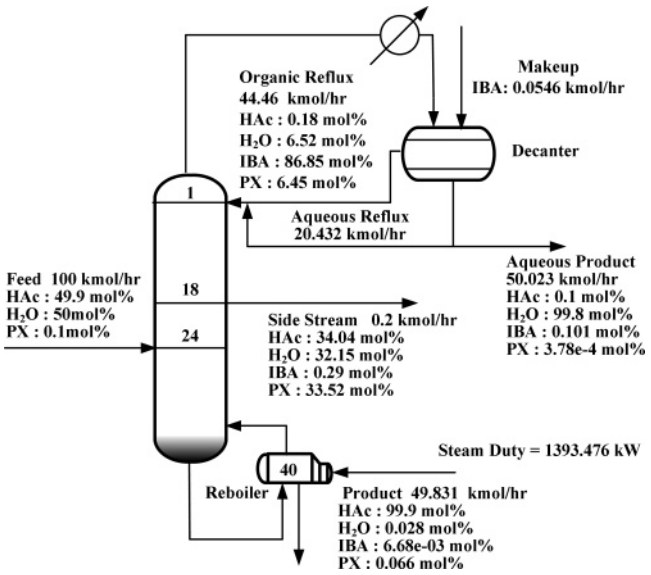

Figure 12. Process configuration with changing feed location (PX impurity system).

design condition with the lowest TAC at another feed tray location. By collecting all the results of all alternative feed tray locations, the overall optimal design condition with the minimized TAC can be obtained. Notice that the TAC formula used is the same as in eq 2.

For the PX impurity system, the final optimized results are summarized in Figure 12 with feed tray location changes from the original ninth stage to a much different location at the 24th stage. The side stream location is also changed from the 21st stage to the 18th stage. Notice also that the side stream flow rate is further reduced from 0.7 to 0.2 kmol/h because a much richer PX can be found inside the column at this location. For the MX impurity system, the results are very similar, with the feed tray location changes from the original ninth stage to a much different location at the 23th stage, the side stream location is also changed from the 21st stage to the 17th stage, and the side stream flow rate is reduced from 0.7 to 0.18 kmol/h. The liquid composition and temperature profiles for the case 3 are shown in Figure 13. The numbers of trays exhibiting phase splitting phenomena are further increased from 21 stages in case 2 to 25 or 24 stages for PX or MX feed impurity cases, respectively.

By comparing Figure 12 with Figure 10, it is found that the reboiler heat duty (for PX system) can be reduced from 1710.80 to 1393.48 KW (an 18.5% reduction). Table 3 shows that the TAC values of the two impurity systems are reduced from $\$559.6 \times 10^3$ to $\$438.3 \times 10^3$ (a 21.7% reduction for the PX system) and from $\$553.1 \times 10^3$ to $\$436.8 \times 10^3$ (a 21.0% reduction for the MX system). The operating costs are also reduced from $\$163.8 \times 10^3$ to $\$133.4 \times 10^3$ (for the PX system) and from $\$161.2 \times 10^3$ to $\$129.3 \times 10^3$ (for the MX system). Hence, by just adding feed tray location as another design variable in the optimization search, significant savings in TAC and operating energy can be realized. This base case design will be used in a follow-up control study to investigate the proper overall control strategy to hold the bottom and top product purities despite feedwater composition changes or the changes in PX or MX impurity in the feed stream.

3.3. Effects of Lowering Bottom Product Specification. From the previous study, the necessity of the side stream in previous design is due to the combinatory effects of assuming 0.1 mol % feed impurity and stringent bottom product specification of 99.9 mol % HAc. Because only 0.1 mol % is allowed in the column bottoms for the remaining components in the system besides HAc, the feed impurity (PX or MX) cannot be designed to completely withdraw from the bottoms even though this impurity is the heaviest component in the system. To investigate an alternative case in which PX or MX can be designed to completely withdraw from the column bottoms while keeping the feed composition the same as in cases 2 or 3, a lower bottom product specification is assumed. This bottom product specification is changed from the original 99.9 mol %

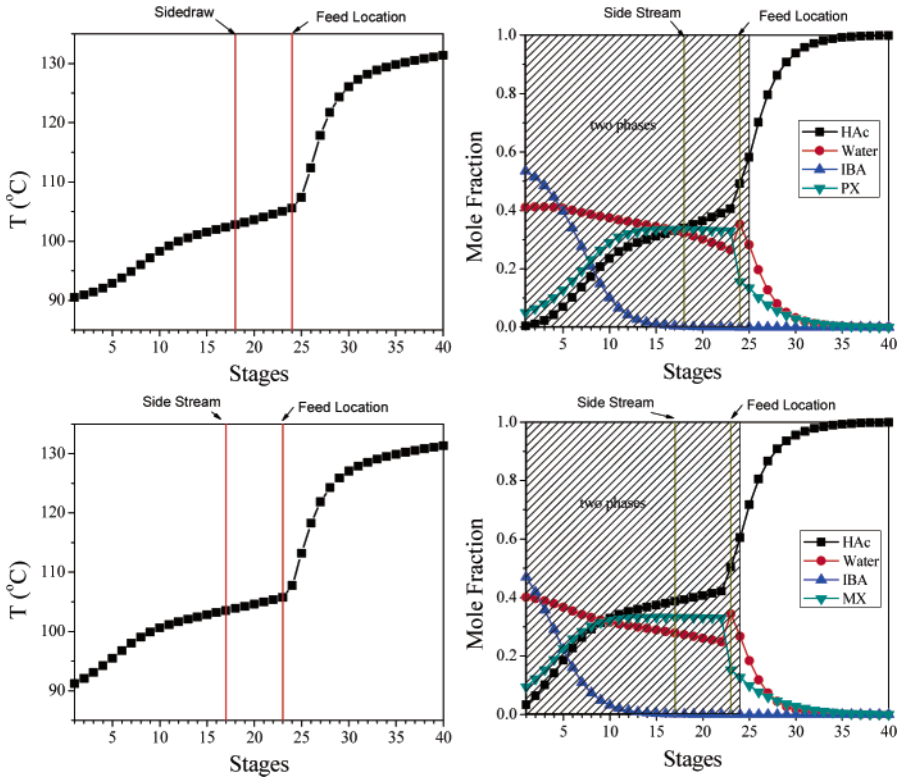

Figure 13. Temperature and liquid composition profiles for PX and MX impurity cases with changing feed location.

Table 4. TAC and Other Results with Lower Bottom Product Specification[a]

	without impurity	MX impurity	PX impurity
	Feed Stage = 9th		
TAC [$1000/year]	362.324 (base case)	532.856 (47.07%)	544.411 (50.26%)
capital cost [$1000/year]	204.879	282.526	285.744
operating cost [$1000/year]	106.087	180.595	183.977
entrainer cost [$1000/year]	51.358	69.735	74.690
reboiler duty [kW]	1107.101	1886.754	1922.142
	Feed Stage = 24th		
TAC [$1000/year]	446.776 (23.31%)	409.156 (12.93%)	410.931 (13.42%)
capital cost [$1000/year]	249.387	229.024	230.814
operating cost [$1000/year]	145.771	127.645	129.315
entrainer cost [$1000/year]	51.618	52.488	50.802
reboiler duty [kW]	1522.331	1332.702	1350.181

[a] Bottom HAc = 99.5 mol %; top HAc = 0.1 mol %; total stages = 36.

HAc to 99.5 mol %. With this assumption of lowering the bottom product specification, the side stream may not be needed because PX or MX can go out of the system from the column bottoms. The specifications of top outlet stream and feed conditions are the same as in previous cases.

Following the design procedure of case 1, the case without impurity also can be established with this lowering of bottom product specification. The result of the optimum search obtains the total stages of 36 and the feed tray location at the ninth stage which is the same as in case 1.

Based on the above base case, changing the feed condition to the case with 0.1 mol % feed impurity by fixing or varying the feed tray location can be studied. Following the optimization procedures of section 3.2.1 and 3.2.2, the optimal results can be found with elimination of the steps containing side stream flow rate and side stream location. The overall results for the comparison are summarized in Table 4. From the table, the TAC values with PX or MX feed impurity by fixed feed tray location in the ninth tray also increase about 50% and the operating costs increase about 70% than the case without impurity. For the lowering bottom product specification cases, the percentage of increase of the reboiler duty is more significant than previous cases which are shown in Table 3. The same tendency for the savings in TAC and operating costs are observed by allowing the feed tray location to vary.

One interesting observation from Table 4 is that TAC will increase 23.31% when moving the feed location from the ninth stage to the 24th stage for the case without feed impurity. Thus, an optimal design layout for both the without-impurity and with-impurity cases cannot be found. If feed stream does not contain PX or MX impurity, the feed location should be placed at the ninth stage. On the other hand, if the feed stream inevitably contains some PX or MX impurity, the feed location should be placed at the 24th stage to save TAC and operating costs.

Another comment for this design of no side stream with lowering of bottom product specification is about the robust design issue. If the feed impurity can be varied in a rather wide range, this design of no side stream is not recommended. The obvious reason is that when the composition of feed impurity is increased to a level where total impurity cannot be balanced with the assumption of complete withdrawal of the

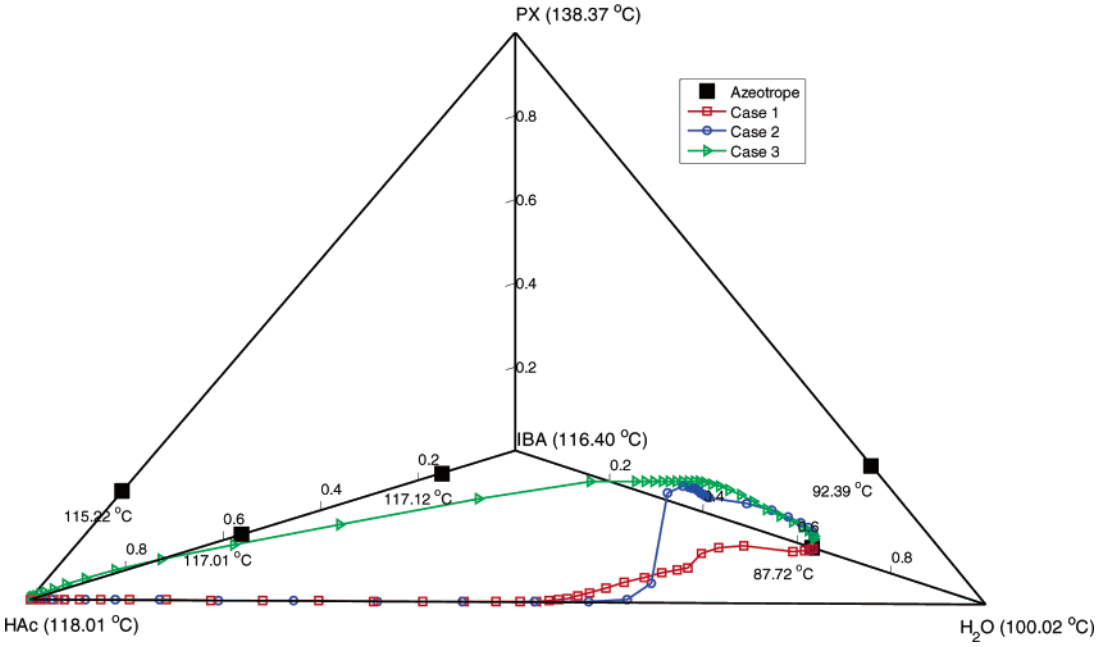

Figure 14. Three-dimensional plot of the four-component system.

impurity through the column bottoms, the bottom product specification cannot be met. Any operating and control strategy trying to hold the bottom product purity at specification will collapse. Thus, for robustness purpose, when feed impurity can be varied in a rather wide range, a side stream should be designed.

4. Distillation Path for Different Design Cases

From the above analysis, the feed tray location is an important design variable in the HAc dehydration process with impurity. To understand the effect of feed tray location on this system, the behaviors and phenomena of column composition profiles are investigated. To simplify the case analyses, the system with PX impurity is selected as an example to demonstrate the results of case 2 and case 3.

In both cases, there are four components in the system. One way to observe the column composition profiles is to draw a three-dimensional plot with four components as in Figure 14. In this figure, the three components of HAc−H_2O−IBA are placed in the bottom of the three-dimensional plot. Therefore, display of the result for case 1 is at the bottom of this figure. In Figure 14 with the squares denoting the column vapor composition profile for case 1, the design principle is met with the column top vapor near the IBA−H_2O azeotrope and the column bottoms toward the pure HAc corner. Notice that the column composition profile avoids the region near the pure water corner which exhibits tangent pinch behavior.

For case 2 with the feed tray location the same as in case 1, the column vapor composition profile is denoted by circles in Figure 14. From this figure, the column top vapor is again near the IBA−H_2O azeotrope; however, it is reached toward that azeotropic point from a different direction with some PX in this top vapor stream. Also notice that the composition profile of case 2 is similar to that of case 1 toward the bottom part of the column. The pure HAc corner is reached from the HAc−H_2O edge.

For case 3, a completely different distillation path of the column profile is observed. The composition profile at the top part of the column is similar to case 2, reaching the IBA−H_2O azeotropic point from the direction with some PX in this top vapor stream. However, the composition profile at the bottom part of the column is completely different than that of case 2. The pure HAc corner is reached from the direction not from the bottom plane but with PX as the major bottom impurity. This can also be found from the stream information in Figure 12. The bottom composition of case 3 contains 0.066 mol % PX and 0.028 mol % H_2O, while the vast majority of the bottom impurity of case 2 is water.

Another way to observe the column composition profile is to use the method by Cruickshank et al.[19] Cruickshank et al.[19] proposed an orthogonal projection that they found to be useful for four-component systems. Wibowo and Ng[20] used the same method to represent LLE data for the visualization of high-dimensional systems. Following the general procedure of a Cruickshank projection, we arrive at the following set of transformed coordinates. The corresponding coordinates are $X_A = x_{HAc} + x_{PX}$ and $X_B = x_{IBA} + x_{PX}$. This set of transformed coordinates has been used to also represent the LLE envelope. For cases 2 and 3 with PX impurity, their Cruickshank projections are shown in parts a and b, respectively, of Figure 15. In these figures, the gray region is the LLE envelope. The region of shaded area inside the gray region is the LLE envelope on the HAc−H_2O−IBA surface.

From the Cruickshank projection of Figure 15, the difference of the column composition profiles of cases 2 and 3 can also be seen. The bottom part of the column profile of case 2 is along the HAc−H_2O edge to the pure HAc. However, for case 3, it goes through another different path richer in PX to the pure HAc corner. This observation can also be seen in Figures 11 and 13. It is noticed that for case 2 the liquid composition profile in the bottom part of the column (from the 23rd stage to the 40th stage) contains almost no PX. However, for case 3 (again from the 23rd stage to the 40th stage), a significant amount of PX can be found in this part of the column. Another observation also related to a different path in Figure 15 is that more stages exhibit liquid−liquid splitting behavior for case 3 (25 stages) compared with case 2 (21 stages).

From the TAC analysis in previous sections, it is demonstrated that the column composition profile following the distillation path with more PX in the bottom part of the column

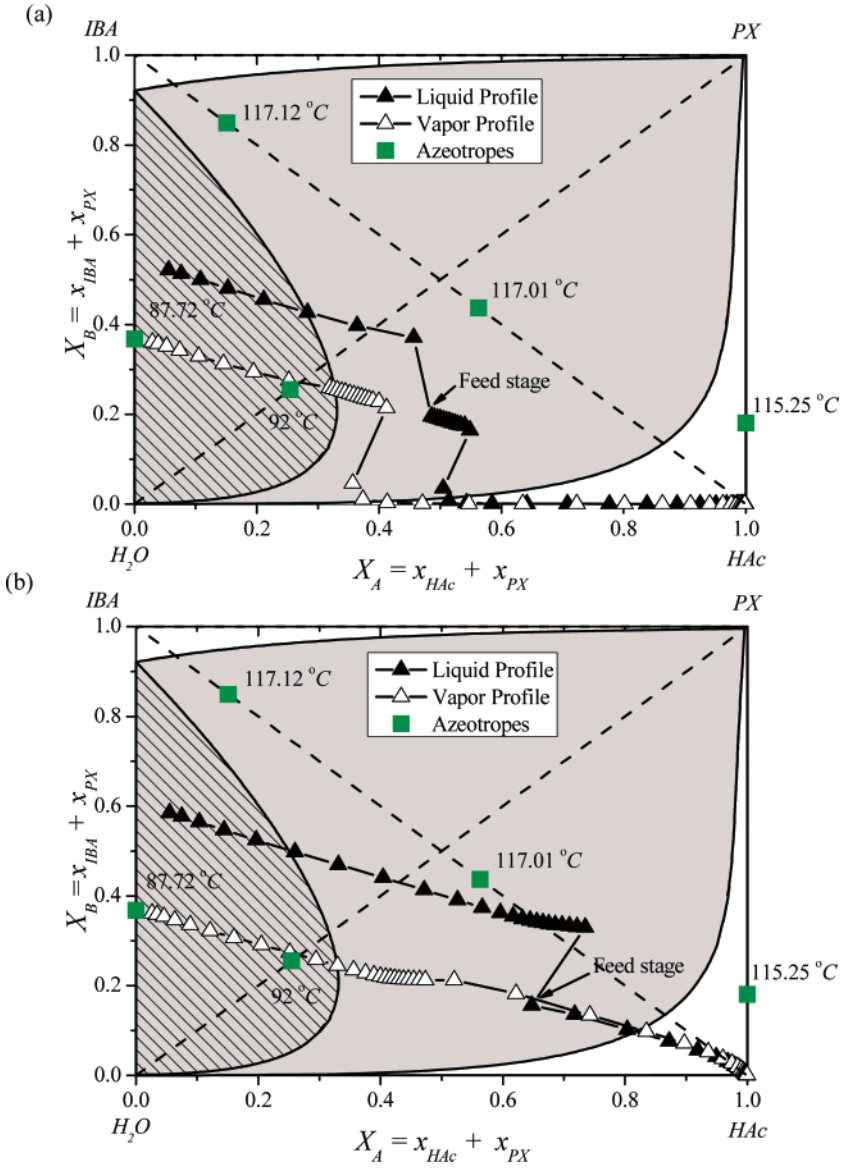

Figure 15. Cruickshank projections with PX impurity: (a) case 2; (b) case 3.

is more favorable in saving TAC and operating costs. This study provides very useful information in terms of how the distillation path inside the column should follow. This unique characteristic of column composition profile should be maintained even though various disturbance changes inevitably could enter the column system.

5. Conclusions

In this paper, the process flow sheets with and without tiny impurity of PX or MX are considered in the optimal design of an acetic acid dehydration column via heterogeneous azeotropic distillation. The simulation results show that dramatic differences in the base case conditions are found by just adding 0.1 mol % PX or MX feed impurity into this column. Over 50% more TAC and operating energy are needed to operate this column with side stream under the "with feed impurity" case. However, by considering the feed tray location as an additional design variable in the optimization search, significant savings in TAC with a reduction of more than 21% can be realized. Note particularly that, with this change of the feed tray location, a significant saving of the reboiler duty with a reduction of more than 18% can also be achieved. The favorable column composition profile should follow the distillation path with more PX in the bottom part of the column. More stages exhibiting liquid−liquid splitting is also observed for this desirable distillation path of column composition profile. This desirable distillation path should be maintained even though various disturbance changes inevitably could enter the column system.

Acknowledgment

This work is supported by the Ministry of Economic Affairs of the R.O.C. under Grant 94-EC-17-A-09-S1-019

Literature Cited

(1) Hindmarsh, E.; Turner, J. A.; Ure, A. M. Process for the production of terephthalic acid. U.S. Patent 5,563,293, Oct 8, 1996.

(2) Lee, F. M.; Lamshing, W.; Wytcherley, R. W. Method and Apparatus for Preparing Purified Terephthalic Acid and Isophthalic Acid from Mixed xylenes. U.S. Patent 6,054,610, April 25, 2000.

(3) Othmer, D. F. Azeotropic Separation. *Chem. Eng. Prog.* **1963**, *59* (6), 67−78.

(4) Pham, H. N.; Doherty, M. F. Design and Synthesis of Heterogeneous Azeotropic Distillations−III. Column Sequences. *Chem. Eng. Sci.* **1990**, *45* (7), 1845−1854.

(5) Tanake, S.; Yamada, J. Graphical Calculation Method for Minimum Reflux Ratio in Azeotropic Distillation. *J. Chem. Eng. Jpn.* **1972**, *5*, 20−26.

(6) Othmer, D. F. Azeotropic Distillation for Dehydrating Acetic Acid. *Chem. Metall. Eng.* **1941**, *40*, 91−95.

(7) Siirola, J. J. An Industrial Perspective on Process Synthesis. In *AIChE Symposium Series*; Biegler, L. T., Doherty, M. F., Eds.; CACHE: Austin, TX, 1995; No. 304, pp 222−233.

(8) Wasylkiewicz, S. K.; Kobylka, L. C.; Castillo, F. J. L. Optimal Design of Complex Azeotropic Distillation Columns. *Chem. Eng. J.* **2000**, *79*, 219−227.

(9) Chien, I. L.; Zeng, K. L.; Chao, H. Y.; Liu, J. H. Design and Control of Acetic Acid Dehydration System via Heterogeneous Azeotropic Distillation. *Chem. Eng. Sci.* **2004**, *59* (21), 4547−4567.

(10) Chien, I. L.; Huang, H. P.; Gau, T. K.; Wang, C. H. Influence of Feed Impurity on the Design and Operation of an Industrial Acetic Acid Dehydration Column. *Ind. Eng. Chem. Res.* **2005**, *44*, 3510−3521.

(11) Gmehling, J. *Azeotropic data*, 2nd ed.; Wiley-VCH: Weinheim, 2004.

(12) Christensen, S. P.; Olson, J. D. Phase Equilibria and Multiple Azeotropy of the Acetic Acid-Isobutyl Acetate System. *Fluid Phase Equilib.* **1992**, *79*, 187−199.

(13) Burguet, M. C.; Montón, J. B.; Muñoz, R.; Wisniak, J. Polyazeotropy in Associating Systems: The 2-Methylpropyl Ethanoate+Ethanoic Acid System. *J. Chem. Eng. Data* **1996**, *41*, 1191−1195.

(14) Hayden, J. G.; O'Connell, J. P. A Generalized Method for Predicting Second Virial Coefficients. *Ind. Eng. Chem. Process Des. Dev.* **1975**, *14*, 209−216.

(15) Jou, F. Y.; Mather, A. E.; Liquid-Liquid Equilibria for Binary Mixtures of Water + Benzene, Water + Toluene, and Water + p-Xylene from 273 K to 458 K. *J. Chem. Eng. Data* **2003**, *48*, 750−752.

(16) Gmehling, J.; Onken, U. *Vapor-Liquid Equilibrium Data Collection*; Dechema: Flushing, NY, 1977.

(17) Tang, Y. T.; Chen, Y. W.; Huang, H. P.; Yu, C. C.; Hung, S. B.; Lee, M. J. Design of Reactive Distillations for Acetic Acid Esterification. *AIChE J.* **2005**, *51*, 1683−1699.

(18) Pöpken, T.; Gmehling, J. Simple Method for Determining the Location of Distillation Region Boundaries in Quaternary Systems. *Ind. Eng. Chem. Res.* **2004**, *43*, 777−783.

(19) Cruickshank, A. J. B.; Haertsch, N.; Hunter, T. G. Liquid-Liquid Equilibrium of Four-Component Systems. *Ind. Eng. Chem.* **1950**, *42*, 2154.

(20) Wibowo, C.; Ng, K. M. Visualization of High-Dimensional Systems via Geometric Modeling with Homogeneous Coordinates. *Ind. Eng. Chem. Res.* **2002**, *41*, 2213−2225.

Received for review July 10, 2006
Revised manuscript received October 18, 2006
Accepted October 23, 2006

IE060883O